UNIVERSITY *of York*

This is a repository copy of *Characterization of the shape-staggering effect in mercury nuclei*.

White Rose Research Online URL for this paper:
https://eprints.whiterose.ac.uk/id/eprint/137498/

Version: Accepted Version

Article:

White Rose
university consortium
Universities of Leeds, Sheffield & York

eprints@whiterose.ac.uk
https://eprints.whiterose.ac.uk/

Mercurial nuclei get back in shape

B. A. Marsh[1,*]**, T. Day Goodacre**[1,2,+]**, S. Sels**[3,+]**, Y. Tsunoda**[4]**, B. Andel**[5]**, A. N. Andreyev**[6]**, N. A. Althubiti**[2]**, D. Atanasov**[7]**, A. E. Barzakh**[8]**, J. Billowes**[2]**, K. Blaum**[7]**, T. E. Cocolios**[2]**, J. G. Cubiss**[6]**, J. Dobaczewski**[6]**, G. J. Farooq-Smith**[2]**, D. V. Fedorov**[8]**, V. N. Fedosseev**[1]**, K. T. Flanagan**[2]**, L. P. Gaffney**[3,9]**, L. Ghys**[3]**, M. Huyse**[3]**, S. Kreim**[7]**, D. Lunney**[10]**, K. M. Lynch**[1]**, V. Manea**[7]**, Y. Martinez Palenzuela**[3]**, P. L. Molkanov**[8]**, T. Otsuka**[3,4,11,12,13]**, A. Pastore**[6]**, M. Rosenbusch**[12,14]**, R. E. Rossel**[1]**, S. Rothe**[1,2]**, L. Schweikhard**[14]**, M. D. Seliverstov**[8]**, P. Spagnoletti**[9]**, C. Van Beveren**[3]**, P. Van Duppen**[3]**, M. Veinhard**[1]**, E. Verstraelen**[3]**, A. Welker**[15]**, K. Wendt**[16]**, F. Wienholtz**[14]**, R. N. Wolf**[7]**, A. Zadvornaya**[3]**, and K. Zuber**[15]

[1]CERN, Geneva, Switzerland
[2]School of Physics Astronomy, The University of Manchester, Manchester M13 9PL, UK
[3]KU Leuven, Instituut voor Kern- en Stralingsfysica, B-3001 Leuven, Belgium
[4]Center for Nuclear Study, University of Tokyo, Hongo, Bunkyo-ku, Tokyo 113-0033, Japan
[5]Department of Nuclear Physics and Biophysics, Comenius University in Bratislava, 84248 Bratislava, Slovakia
[6]University of York, Department of Physics, YO10 5DD, York, UK
[7]Max-Planck-Institut für Kernphysik, Saupfercheckweg 1, 69117 Heidelberg, Germany
[8]Petersburg Nuclear Physics Institute (PNPI), NRC Kurchatov Institute, Gatchina 188300, Russian Federation
[9]School of Engineering and Computing, University of the West of Scotland, High Street, Paisley, PA1 2BE, UK
[10]CSNSM-IN2P3-CNRS, Universite Paris-Sud, 91406 Orsay, France
[11]Department of Physics, University of Tokyo, Hongo, Bunkyo-ku, Tokyo 113-0033, Japan
[12]RIKEN Nishina Center, 2-1 Hirosawa, Wako, Saitama 351-0198, Japan
[13]National Superconducting Cyclotron Laboratory,Michigan State University, East Lansing, Michigan 48824, USA
[14]Ernst-Moritz-Arndt-Universität, Institut für Physik, 17487 Greifswald, Germany
[15]Technische Universität Dresden, 01069 Dresden, Germany
[16]Johannes Gutenberg Universität 55099 Mainz, Germany
*bruce.marsh@cern.ch
+these authors contributed equally to this work

ABSTRACT

Atomic nuclei exhibit single-particle and collective degrees of freedom, making them susceptible to variations in size and shape when adding or removing nucleons. The rare cases where dramatic changes in shape occur with the removal of only a single nucleon are key for pinpointing the components of the nuclear interaction driving nuclear deformation. Laser spectroscopy probes the nuclear charge distribution, revealing attometer-scale variations and highlighting sensitivity to the proton (Z) and neutron (N) configurations of the nucleus. The lead isotopes, which possess a closed proton shell ($Z = 82$), are spherical and steadily shrink with decreasing N. A surprisingly different story was observed for their close neighbours, the mercury isotopes ($Z = 80$) almost half a century ago[1,2]: Whilst the even-mass isotopes follow the trend seen for lead, the odd-mass isotopes ^{181,183,185}Hg exhibit a striking increase in charge radius. This dramatic 'shape staggering' between even- and odd-mass isotopes remains a unique feature of the nuclear chart.

Here we present the extension of laser spectroscopy results that reach ^{177}Hg. An unprecedented combination of state-of-the-art techniques including resonance laser ionization, nuclear spectroscopy and mass spectrometry, has established ^{181}Hg as the shape-staggering endpoint. Accompanying this experimental tour de force, recent computational advances incorporating the largest valence space ever used have been exploited to provide Monte-Carlo Shell Model calculations, in remarkable agreement with the experimental observations. Thus, microscopic insight into the subtle interplay of nuclear interactions that give rise to this phenomenon has been obtained, identifying the shape-driving orbitals. Although shape staggering in the mercury isotopes is a unique and localized feature in the nuclear chart, the underlying mechanism that has now been uncovered nicely describes the duality of single-particle and collective degrees of freedom in atomic nuclei.

Atomic nuclei, comprising protons and neutrons, display a rich array of quantum phenomena. These complex many-body systems obey the Pauli exclusion principle which dictates a shell-like structure, akin to Bohr's model of the atom. In the vicinity of closed shells, at the 'magic numbers'of $Z, N = 8, 20, 28, 50, 82$ and $N = 126$, the nuclear wavefunction is dominated by the last few particles (or holes) and excitations thereof. In contrast to this single-particle nature,
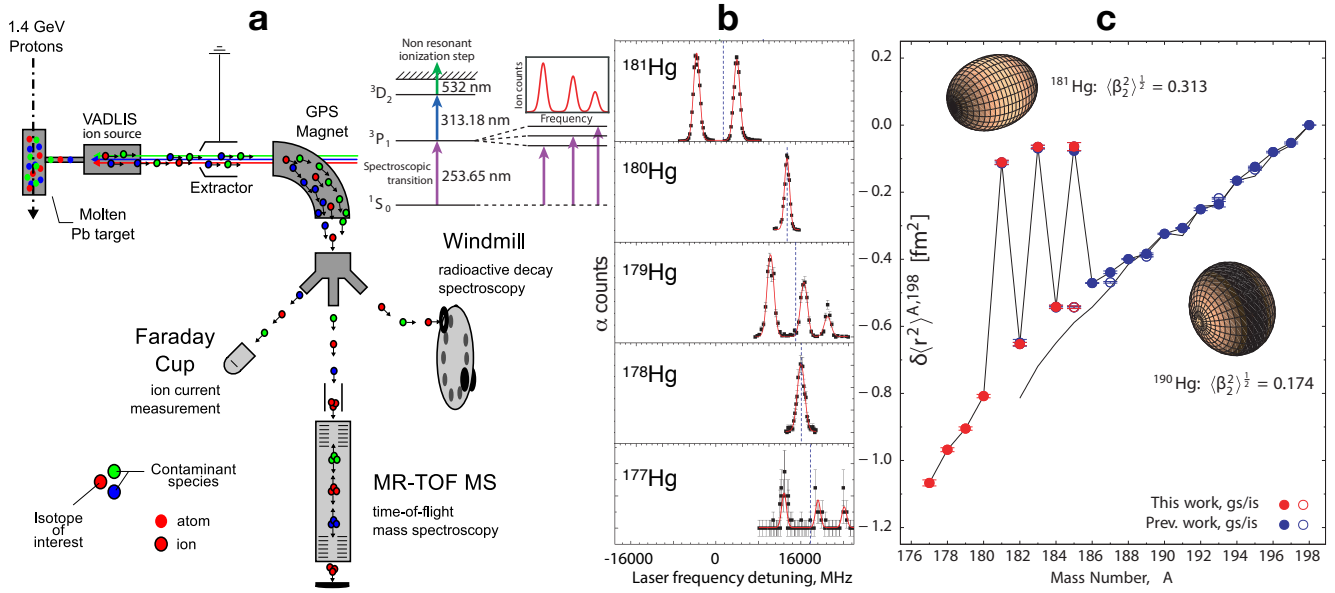
Figure 1. Schematic of the in-source resonance ionization spectroscopy method for the study of radiogenic mercury isotopes (see Methods) (a): mercury isotopes are produced by proton-induced nuclear reactions in a molten lead target. The vapor effuses into the anode volume of the VADLIS ion source[3] where the atoms are ionized using a 3-step resonance photo-ionization scheme (inset). The ions are extracted as a mono-energetic beam at 30 keV. The isotope of interest is selected using the general-purpose mass separator (GPS) and directed towards the most appropriate of the three detection systems depicted. By scanning the 1st-step laser wavelength, the isotope shift (IS) and hyperfine structure (HFS) is studied (b). The isotope shifts are used to calculate the changes in mean-squared charge radii $\delta\langle r^2 \rangle$ with respect to $N = 126$ along the isotopic chain (c). The results of this study appear as red circles. $^{177-180}$Hg are new measurements, while $^{181-185}$Hg were re-measured and the data points overlap with those of the literature values, as can also be seen by the close agreement between values in Table 1. The error bars indicate the statistical uncertainty corresponding to the measurement precision. The scaling uncertainties arising from the indeterminacy of the F factor (7%[4]) and the Specific Mass Shift, M_{SMS} are discussed in the Methods section and provided in Table 1 (see Supplementary Information linked to the on-line version). The additional black line illustrates the previously measured quasi-spherical trend of the lead nuclei[5].

collective behaviour appears away from the closed shells, as increased nucleon-nucleon correlations drive the minimum-energy configuration of the nucleus to deformation. Consequently, the ground-states of most isotopes in the nuclear chart have non-spherical shapes, the most common being the prolate (rugby-ball) shape. Different shapes, corresponding to alternative nucleon configurations, can coexist within the same nucleus[6,7]. It remains a challenge to present the full picture of the underlying microscopic origin of this phenomenon.

Optical spectroscopy is able to measure subtle shifts in the energy of the atomic electron levels, arising from changes in the charge distribution of the nucleus[8]. Along the isotopic chain of a given element, this effect is known as the isotope shift. From this, the change in mean-square charge radius, $\delta\langle r^2 \rangle$, can be extracted in a nuclear-model independent way. Similarly, the hyperfine splitting of the electronic levels gives direct access to the nuclear properties: spin (I), magnetic dipole (μ) and electric quadrupole (Q) moments. Such measurements are therefore a sensitive and direct probe of the valence particle configuration and changes in nuclear

size or deformation as a result of the addition, removal, and consequential redistribution of nucleons.

The radioactive isotopes in the lead region have been the subject of a variety of optical spectroscopy studies for several decades. An intensified interest in this region was sparked by the study of the mercury isotopic chain in which a sudden and unprecedented increase in charge radius was observed for ^{185}Hg, ^{183}Hg and ^{181}Hg[1,2]. For the heavier mercury isotopes the changes in charge radii mirror those of lead[5]: steadily shrinking with decreasing N. This seminal discovery of shape-staggering between odd and even mercury isotopes is unparalleled elsewhere in the nuclear chart and was key to establishing the idea of shape coexistence at low excitation energy[7,9]. A plethora of studies on the excited states of these nuclei[10,11] provided a further substantial insight into shape-coexistence, complementing the laser spectroscopy studies of ground and isomeric-states. However, to acquire a full understanding of this phenomenon two challenges remain:

Understanding the nature of this spectacular occurance requires its precise localisation by probing even more neutron-deficient systems, which were experimentally inaccessible.

Likewise, theoretical solutions have been thwarted by the enormous computational requirements of a fully microscopic, many-body calculation of such heavy systems.

In this Letter we report breakthroughs on both fronts that now provide explanations of the underlying mechanism and localized nature of shape coexistence:

1. The combination of state-of-the-art radioisotope production and detection techniques (see Figure 1**a**) at the CERN-ISOLDE radioactive ion beam facility[12], extending laser spectroscopy measurements to four lighter mercury isotopes; and

2. The exploitation of recent advances in computational physics to perform Configuration-Interaction Monte Carlo Shell Model (MCSM)[13] calculations with the largest model spaces to date.

The new experimental scheme is illustrated in Fig. 1**a** with the recorded laser spectra shown in Fig.1**b** and resulting charge-radii data in Fig. 1**c**.

Ground-state charge radii and magnetic moments were studied by performing resonance ionization spectroscopy on the mercury isotopes with unprecedented sensitivity, reaching as far as ^{177}Hg, an isotope with a half-life of only 127 milliseconds and a production rate as low as one ion per minute.

The isotope shifts measured relative to ^{198}Hg and the deduced changes in mean-square charge radii and moments for $^{177-185}$Hg are presented in Table 1 (see Supplementary Information linked to the on-line version). The changes in mean-square charge radii of mercury isotopes combined with those of the lead isotopes[5] are shown relative to $N = 126$ in Figure 1**c**. In addition to confirming the earlier results, these new data firmly prove that the dramatic shape staggering is a local phenomenon and that the odd-mass mercury isotopes return to sphericity at $A = 179$ ($N = 99$).

In order to pinpoint the microscopic origin of this observation, we performed large-scale numerical simulations for the quantum many-body problem using a MCSM method. Heavy nuclei such as the mercury isotopes are beyond the limit of conventional Configuration Interaction (CI) calculations for protons and neutrons interacting through nuclear forces. However, using the MCSM method and the most advanced computers has allowed us to reach this region for the first time, redefining the state of the art of CI calculations for atomic nuclei. Calculations were performed for the ground and the lowest excited states in $^{177-186}$Hg with spin and parity corresponding to the experimental ground-state values of the nuclei considered: 0^+ for the even-mass isotopes, $1/2^-$ for ^{181,183,185}Hg and $7/2^-$ for ^{177,179}Hg. Also the $13/2^+$ long-lived isomer in ^{185}Hg was examined. The MCSM provides the eigen wavefunction from which the magnetic dipole and electric quadrupole moments, and the shape parameters (β_2, γ) are calculated[14]. In turn, the shape parameters are used to obtain the mean-square charge radius (see Methods). For all these states, the changes in mean-square charge radii relative to the ground state of ^{186}Hg are presented as shaded boxes

in Figure 2**a**. The height of the shaded box is related to the spread of the quantum fluctuations of the MCSM eigenstates (see Methods). The figure shows that for every mercury isotope, only one state can be identified whose calculated $\delta \langle r^2 \rangle$ is in agreement with experiment. For the odd-mass nuclei this identification is confirmed by the agreement between the calculated and measured magnetic moments, as shown in Figure 2**b**. Furthermore, with the exception of ^{181}Hg and in spite of the limited number of basis vectors used, the selected MCSM states correspond indeed to the ground states in the calculations. The remarkable agreement with the experimental data that has been achieved reinforces our confidence in ability of these MCSM calculations to reveal the discrete changes in the nuclear configuration that drive shape coexistence in this region. We therefore gain an insight into the underlying mechanism responsible for the sudden appearance and disappearance of the uniquely-pronounced shape staggering in the mercury isotopes.

The MCSM enables us to examine the microscopic composition of each MCSM state in terms of the occupancy of the proton and neutron orbitals (see Figure 2**c**). The most striking differences between the deformed $1/2^-$ states in ^{181,183,185}Hg and the other near-spherical states are found in the nucleon-occupancy of two orbitals: the proton $1h_{9/2}$ situated above the $Z = 82$ closed shell and the neutron $1i_{13/2}$ midshell between $N = 82$ and $N = 126$. The strongly deformed $1/2^-$ states of ^{181,183,185}Hg exhibit large and constant values (~ 8) of the neutron $1i_{13/2}$ occupation number, as well as a sizable promotion of 2 to 3 protons across the $Z = 82$ magic shell gap to the $1h_{9/2}$ orbit.

This abrupt and significant reconfiguration of the nucleons originates not only from the quadrupole component of the nucleon-nucleon (NN) interaction, known to be responsible for inducing deformation in atomic nuclei, but also in the monopole component. The strong attractive nature of the latter, specifically between the proton $1h_{9/2}$ orbital and neutron $1i_{13/2}$ orbital, results in an additional lowering of the binding energy[14]. If this energy gain, combined with that of the quadrupole deformation, exceeds the energy needed to create particle-hole excitations then the deformed state becomes the ground state.

It is thus the combined action of the monopole interaction, whose effect depends linearly on the orbital occupancy numbers, and the quadrupole interaction, that follows a quadratic dependence with a maximum when an orbital is half-filled (i.e. 7 neutrons in the $1i_{13/2}$ orbital) that delineates the deformed region for the mercury isotopic chain between $N = 101$ and $N = 105$. For even-N mercury isotopes, the pairing correlation that exists for the spherical shape produces sufficient binding energy because of the high level density, whereas this is suppressed in odd-N isotopes due to blocking of the unpaired neutron. The strongly deformed state, assisted by the combined monopole and quadrupole effect, therefore becomes the ground state. Thus, the observed shape staggering is due to a subtle competition between these two
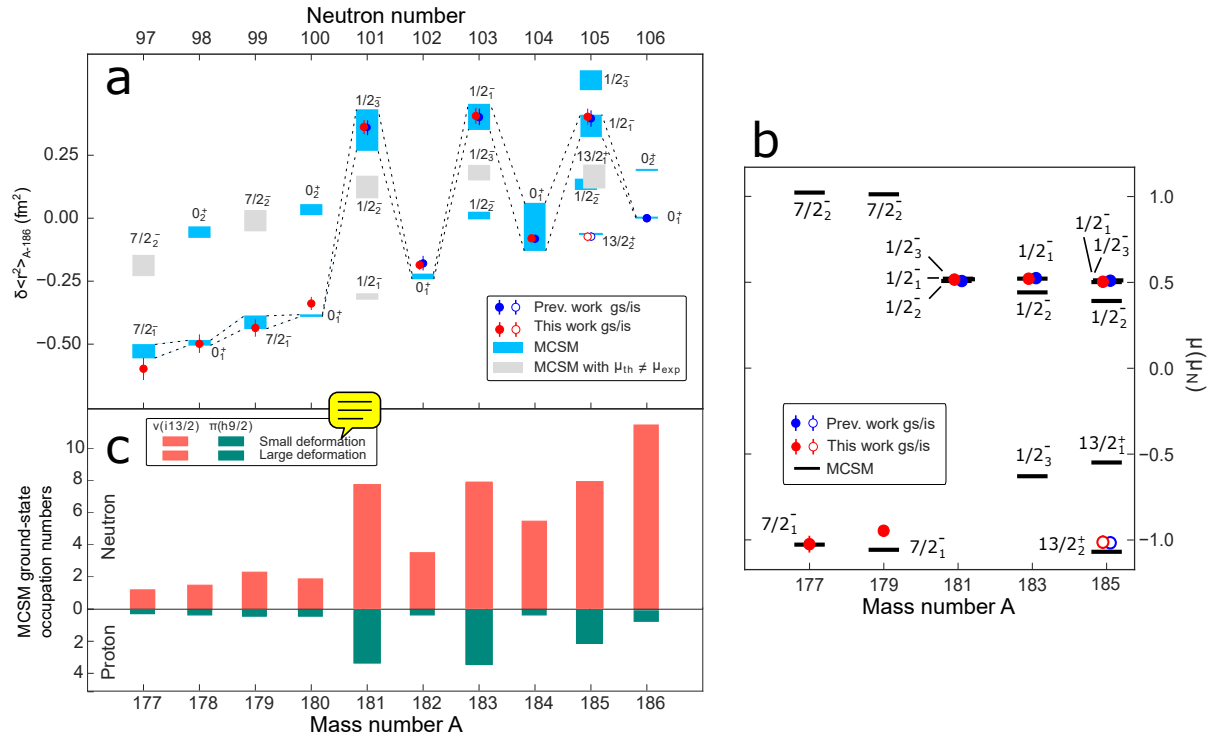
Figure 2. **a**: The upper left panel shows $\langle r^2 \rangle$ relative to that of the ground state of ^{186}Hg. Red points are experimental data from this experiment. They include the combined statistical and systematic uncertainties quoted in Table 1. Blue points refer to literature values from[4]. The shaded boxes indicate radii corresponding to the MCSM eigenstates labeled by their respective spin J, parity π and energetic ordering i as J_i^π. The gray areas show MCSM eigenstates for which the calculated magnetic moment differs from measured value. **b**: Comparison of the calculated and experimental magnetic moments for different states in the odd-mass mercury isotopes. **c**: The occupation numbers of the neutron $i_{13/2}$ orbit and the proton $h_{9/2}$ orbit for the states displayed by the blue connected areas in panel **a** (these are the experimentally-observed ground-states). The deviation of the three strongly prolate deformed states at $A = 181, 183, 185$ from the general occupancy trend is evident.

shapes, which are different in terms of their many-body configuration. The shape staggering effect manifests characteristic features of a quantum phase transition[15–17]: In a given nucleus, different phases - a near spherical and a strongly deformed nuclear shape - appear at almost the same energy without mixing. By making small changes in the control parameter, which in this case is the neutron number, the system alternates between the two phases. In the case of the mercury chain, this observation, which resembles a critical phenomenon in phase transitions, happens six times. This unique feature is now quantitatively understood through the MCSM calculations, highlighting the importance of the simultaneous multiple excitations to the proton $1h_{9/2}$ and neutron $1i_{13/2}$ orbitals[14]. In this picture, because of the major role of the neutron $1i_{13/2}$ orbital in driving the large quadrupole deformation, this effect can only dominate close to neutron number N=103. By delineating the region of shape staggering our new data provides the neccessary information to support this picture.

~~In~~ ~~summary, the lightest mercury isotopes return towards~~ ~~sphericity and the region of shape staggering is delineated~~

~~between $N = 101$ and $N = 105$. Its~~ underlying microscopic ~~origin has been identified through MCSM calculations~~ as ~~an~~ ~~abrupt and significant reconfiguration of the nucleon orbital~~ ~~occupancies.~~

The extension of the MCSM calculations to other states should allow further comparisons with available experimental information on the different band structures identified in nuclear spectroscopy studies. This will be complemented by information from Coulomb excitation and nucleon transfer experiments on the ground and isomeric states, now possible using post-accelerated radioactive ion beams[18].

In this work we have uncovered the general mechanism that links different features in various locations of the nuclear chart, thereby providing a deeper understanding of the structure of atomic nuclei in general.

Methods summary

The experiment was performed at the CERN-ISOLDE isotope separator facility using the technique of in-source resonance ionization spectroscopy[19], as depicted in Figure 1.

~~Mercury isotopes were produced by spallation of lead nuclei in a liquid target using up to 1 μA of 1.4 GeV protons from the CERN PS Booster Synchrotron. The radiogenic mercury vapor diffuse into the anode cavity of the Versatile Arc Discharge and Laser Ion Source (VADLIS) where~~ resonance ionization spectroscopy was performed by wavelength-tuning of the 254 nm first-step transition ($6s^2\ ^1S_0 \rightarrow 6d6p\ ^3P_1)^{\circ}$ of the 3-step ionization scheme for Hg^+ ion production (Figure 1**a** inset)[20].

~~The ion beam was mass separated using a magnetic dipole spectrometer, set to transmit a chosen isotope of interest to the most suitable of~~ three detection systems, depending on the beam intensity, purity, decay mode and half-life of the species: the ISOLDE Faraday cup (>100 fA); the ISOLTRAP MR-ToF MS[21] (isobar separated ion counting of longer lived isotopes); or the Windmill decay spectroscopy setup (for efficient and selective detection of alpha-decaying isotopes). Laser spectra were obtained for all isotopes from $^{185-177}$Hg. Isotope shifts, relative to the reference isotope ^{198}Hg, and hyperfine parameters were measured. From these observables, the changes in mean-square charge radii together with spins and magnetic moments were deduced.

Large-scale Monte Carlo shell-model calculations (MCSM) were performed with neutron-neutron and proton-proton interactions taken from[22] and with the proton-neutron interaction taken from[23]. ~~Single-particle energies were varied smoothly as functions of Z and N between the respective values of doubly magic ^{132}Sn and ^{208}Pb. The Hamiltonian was fixed and kept throughout this study. Effective charges for protons and neutrons were used, with their actual values being 1.6e and 0.6e respectively, together with a spin quenching factor of 0.9. The model space in which the nucleons interact are 11 proton orbits from $1g_{7/2}$ up to $1i_{13/2}$ and 13 neutron orbits from $1h_{9/2}$ up to $1j_{15/2}$, corresponding to the largest scale MCSM calculation ever performed.~~

Methods

Mercury isotope production

The experiment was performed at the CERN-ISOLDE isotope separator facility. Neutron deficient mercury isotopes were produced by proton-induced spallation of lead nuclei: a molten lead target was bombarded with protons from the CERN Proton Synchroton booster at an energy of 1.4 GeV. The proton beam intensity (1×10^{13} protons per pulse, up to 1 μA averaged current) and bunched proton extraction was optimized to enhance the release of short-lived isotopes from the liquid target whilst reducing the likelihood of a mechanical failure due to shockwaves generated by the proton impact[24,25]. A temperature-controlled spiral chimney enables effusion of the mercury vapor towards the ion source cavity whilst ensuring the required suppression, by condensation, of less volatile species such as lead. The mercury atoms effuse into the anode cavity of a FEBIAD-type ion source, referred to as the VADLIS (Versatile Arc Discharge and Laser Ion Source)[3]. For this experiment the laser beams from the Resonance Ionization Laser Ion Source (RILIS)[26] setup were directed into the FEBIAD anode cavity through the 1.5 mm ion extraction aperture. The lasers were tuned to the 3-step resonance ionization scheme for mercury (Figure 1**a** inset), resulting in laser-ionization of mercury only. For the first time during on-line operation, the ion source was operated in the newly-established RILIS-mode[3], whereby the anode voltage is reduced to several volts, whilst the cathode heating and ion source magnetic field strength are optimized for laser-ion survival and extraction. In this case, no electron impact ionization occurs, and the laser-ionized Hg^+ beam purity is maximized. The ion source efficiency remains similar to that of standard FEBIAD operation with electron-impact ionization (estimated to be several percent). Mercury ions leaving the anode exit aperture are subject to the 30 kV potential difference between the ion source aperture and the grounded extraction electrode. The resulting mono-energetic beam of mercury ions was then passed through a magnetic dipole mass separator, which has sufficient resolution for the selection of the atomic mass of interest for transmission to the detection system, but is not capable of separating isobars.

Laser spectroscopy and signal identification

To extend our reach beyond the range of previously studied mercury isotopes, it was necessary to use the most sensitive laser spectroscopy method available at ISOLDE: in-source resonance ionization spectroscopy. As the name implies, this approach makes use of the initial ion creation process for performing laser spectroscopy, by wavelength-tuning of one of the lasers used in the resonance ionization scheme, which directly influences the ionization efficiency of the element of interest. For this work the 254 nm first-step transition ($6s^2\ ^1S_0 \rightarrow 6d6p\ ^3P_1)^{\circ}$ of the ionization scheme was used for spectroscopy since its sensitivity to nuclear variations results in a well-resolved hyperfine structure even in the high-temperature ($\approx$1800 °C) Doppler-broadening dominated environment of the ion source cavity. The 254 nm light required was generated by third-harmonic generation from the output of a Ti:Sapphire laser, operating in the dual etalon scanning mode (fundamental linewidth of 0.8 GHz)[27]. While operating the ion source in RILIS-mode, this laser was scanned in a stepwise manner and at each frequency step the ion rate was recorded using the most suitable of the three detection methods available. Depending on the intensity, purity, lifetime or decay mode of the beam at a chosen mass, the ion beam was directed to one of the three detection systems depicted in Figure 1**a**: The ISOLDE Faraday cup, for ion current measurement above 100 fA; the ISOLTRAP MR-ToF MS, for isobar-separated ion counting of longer lived isotopes with a resolving power of $M/\Delta M \approx 300000$[28,29]; or the Windmill decay spectroscopy setup (for efficient detection of alpha-decaying isotopes). Laser scans were obtained for all $^{177-186}$Hg ground states. The isotope shifts were determined relative to ^{198}Hg. A total of 17 ^{198}Hg reference scans were recorded periodically during the experiment.

Monte Carlo Shell Model Calculations

The Monte Carlo Shell Model (MCSM) calculation is one of the most advanced computational methods that can be applied for nuclear many-body systems. This work represents the largest ever MCSM calculations, performed on massively parallel supercomputers, including the K computer in Kobe, Japan. Exploiting the advantages of quantum Monte-Carlo, variational and matrix-diagonalization methods, this approach circumvents the diagonalization of a $> 2 \times 10^{42}$-dimensional Hamiltonian matrix. Using the doubly-magic ^{132}Sn nucleus as an inert core, 30 protons and up to 24 neutrons were left to actively interact in an exceptionally large model space as compared to conventional CI calculations. Single-particle energies were set to be consistent with single-particle properties of ^{132}Sn and ^{208}Pb with smooth changes as functions of Z and N. All nucleons interact through effective NN interactions adopted from the frequently-used ones provided by[22,23]. The Hamiltonian was thus fixed and kept throughout this study. The model space in which the nucleons interact are 11 proton orbits from $1g_{7/2}$ up to $1i_{13/2}$ and 13 neutron orbits from $1h_{9/2}$ up to $1j_{15/2}$. Calculations were performed utilizing effective charges for protons and neutrons, with their actual values being 1.6e and 0.6e, respectively and a spin quenching factor of 0.9. The MCSM eigenstate is represented as a superposition of MCSM basis vectors with the appropriate projection onto spin and parity. Each MCSM basis vector is a Slater determinant formed by mixed single-particle states, where the mixing amplitudes are optimized by quantum Monte-Carlo and variational methods. This Slater determinant has intrinsic quadrupole moments, which can be expressed in terms of a set of β_2 and γ deformation parameters. Using the effective charges and spin quenching factor, we reproduce the electric quadrupole moments of ^{177,179}Hg[30] and the magnetic dipole moments of the odd-mass mercury isotopes (see Figure 2**b**). The combined effect of the monopole interaction, whose effect depends linearly on the orbital occupancy numbers, and the quadrupole interaction, that contains a quadratic dependence with a maximum when an orbital is half-filled, causes the observed shape staggering. Specifically the strong attractive monopole matrix element between proton $h_{9/2}$ and neutron $i_{13/2}$ orbtials (-0.35 MeV) compared to an average value of -0.2 MeV for the other orbitals considered, localizes the observed phenomena around $N = 103$[14]. This is due to the similarity in radial wave functions and the coherent sizable effect of the tensor force[23].

Using the effective charges, the quadrupole moments for each MCSM basis vector can be obtained. These can be converted into the standard ellipsoidal nuclear shape parameters β_2 (deformation strength) and γ (deformation shape)[31]. One of the strengths of the MCSM is the ability to link the basis vectors onto the Potential Energy Surface (PES) deduced using the same NN interaction. The T-plot[14,32] was introduced in order to indicate the individual MCSM basis vectors using β_2 and γ as partial coordinates on the PES.
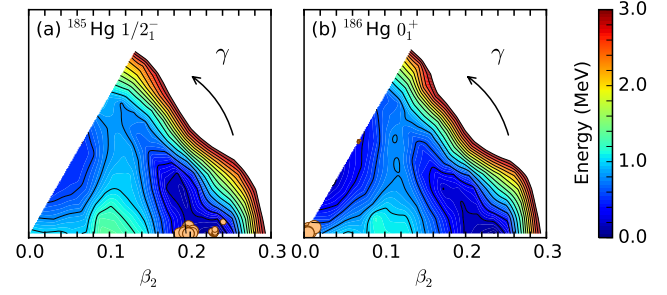
Figure 3. T-plot examples for two different states in ^{185,186}Hg, with large and small deformation respectively. The corresponding β_2 and γ shape parameters of the main contributing MCSM basis vectors are denoted by the yellow circles.

Figure 3 displays example T-plots for ^{185,186}Hg. The importance of each MCSM basis vector is evaluated in terms of the probability amplitude in the eigenstate of interest, and is shown by the size of the circle: larger circles representing major MCSM basis vectors, whilst smaller circles imply a less relevant contribution to this particular eigenstate. In the T-plot, clustering of the circles is observed for spherical (^{186}Hg) and prolate shapes (^{185}Hg).

In order to compare the $\delta\langle r^2\rangle$ from the isotope shift measurements to the β_2 deduced from the MCSM calculations, the following standard procedure was used:

$$\langle r^2 \rangle = \langle r^2 \rangle_{\text{DM}} \left(1 + \frac{5}{4\pi} \langle \beta_2 \rangle^2 \right) \tag{1}$$

$$\delta \langle r^2 \rangle_{A-186} = \langle r^2 \rangle - \langle r^2 \rangle_{186} \tag{2}$$

where $\langle r^2 \rangle_{\text{DM}}$ refers to the droplet model mean square charge radius for which the most-used parametrization of Berdichevsky and Tondeur[33] is adopted. Following this procedure, the influence of γ is negligible.

The calculated $\delta\langle r^2\rangle$, shown in Fig. 2a, are indicated by shaded boxes. The height of the box is determined by the distribution of the circles in the T-plot with respect to β_2 and represents the spread of the quantum fluctuations of the MCSM eigenstates.

Data availability

The data that support the findings of this study are available from the corresponding author upon reasonable request.

References

1. Bonn, J., Huber, G., Kluge, H.-J., Kugler, L. & Otten, E. Sudden change in the nuclear charge distribution of very light mercury isotopes. *Phys. Lett. B* **38**, 308–311 (1972). URL https://doi.org/10.1016%2F0370-2693%2872%2990253-5. DOI 10.1016/0370-2693(72)90253-5.

2. Kühl, T. *et al.* Nuclear shape staggering in very neutron-deficient Hg isotopes detected by laser spectroscopy. *Phys. Rev. Lett.* **39**, 180–183 (1977). URL https://doi.org/10.1103%2Fphysrevlett.39.180. DOI 10.1103/physrevlett.39.180.

3. Day Goodacre, T. *et al.* Blurring the boundaries between ion sources: The application of the RILIS inside a FEBIAD-type ion source at ISOLDE. *Nucl. Instruments Methods Phys. Res. Sect. B: Beam Interactions with Mater. Atoms* **376**, 39–45 (2016). URL https://doi.org/10.1016%2Fj.nimb.2016.03.005. DOI 10.1016/j.nimb.2016.03.005.

4. Ulm, G. *et al.* Isotope shift of ^{182}Hg and an update of nuclear moments and charge radii in the isotope range ^{181}Hg-^{206}Hg. *Zeitschrift fur Physik A At. Nucl.* **325**, 247–259 (1986). URL https://doi.org/10.1007%2Fbf01294605. DOI 10.1007/bf01294605.

5. Witte, H. D. *et al.* Nuclear charge radii of neutron-deficient lead isotopes beyond $n = 104$ midshell investigated by in-source laser spectroscopy. *Phys. Rev. Lett.* **98** (2007). URL https://doi.org/10.1103%2Fphysrevlett.98.112502. DOI 10.1103/physrevlett.98.112502.

6. Andreyev, A. N. *et al.* A triplet of differently shaped spin-zero states in the atomic nucleus ^{186}Pb. *Nat.* **405**, 430–433 (2000). URL https://doi.org/10.1038%2F35013012. DOI 10.1038/35013012.

7. Wood, J. L. & Heyde, K. A focus on shape coexistence in nuclei. *J. Phys. G: Nucl. Part. Phys.* **43**, 020402 (2016). URL https://doi.org/10.1088%2F0954-3899%2F43%2F2%2F020402. DOI 10.1088/0954-3899/43/2/020402.

8. Campbell, P., Moore, I. & Pearson, M. Laser spectroscopy for nuclear structure physics. *Prog. Part. Nucl. Phys.* **86**, 127–180 (2016). URL https://doi.org/10.1016%2Fj.ppnp.2015.09.003. DOI 10.1016/j.ppnp.2015.09.003.

9. Heyde, K. & Wood, J. L. Shape coexistence in atomic nuclei. *Rev. Mod. Phys.* **83**, 1467–1521 (2011). URL https://doi.org/10.1103%2Frevmodphys.83.1467. DOI 10.1103/revmodphys.83.1467.

10. Wrzosek-Lipska, K. & Gaffney, L. P. Unique and complementary information on shape coexistence in the neutron-deficient Pb region derived from coulomb excitation. *J. Phys. G: Nucl. Part. Phys.* **43**, 024012 (2016). URL https://doi.org/10.1088%2F0954-3899%2F43%2F2%2F024012. DOI 10.1088/0954-3899/43/2/024012.

11. Julin, R., Grahn, T., Pakarinen, J. & Rahkila, P. In-beam spectroscopic studies of shape coexistence and collectivity in the neutron-deficient $z \approx 82$ nuclei. *J. Phys. G: Nucl. Part. Phys.* **43**, 024004 (2016). URL https://doi.org/10.1088%2F0954-3899%2F43%2F2%2F024004. DOI 10.1088/0954-3899/43/2/024004.

12. Borge, M. J. G. & Blaum, K. Focus on Exotic Beams at ISOLDE: A Laboratory Portrait. *J. Phys. G: Nucl. Part. Phys.* **45**, 010301 (2017). URL https://doi.org/10.1088%2F1361-6471%2Faa990f. DOI 10.1088/1361-6471/aa990f.

13. Otsuka, T., Honma, M., Mizusaki, T., Shimizu, N. & Utsuno, Y. Monte carlo shell model for atomic nuclei. *Prog. Part. Nucl. Phys.* **47**, 319 – 400 (2001). URL http://www.sciencedirect.com/science/article/pii/S0146641001001570. DOI https://doi.org/10.1016/S0146-6410(01)00157-0.

14. Otsuka, T. & Tsunoda, Y. The role of shell evolution in shape coexistence. *J. Phys. G: Nucl. Part. Phys.* **43**, 024009 (2016). URL https://doi.org/10.1088%2F0954-3899%2F43%2F2%2F024009. DOI 10.1088/0954-3899/43/2/024009.

15. Sachdev, S. *Quantum Phase Transitions - Second Edition* (Cambridge University Press, 2011).

16. Carr, L. D. *Understanding Quantum Phase Transitions* (Crc Press Inc., 2010).

17. Togashi, T., Tsunoda, Y., Otsuka, T. & Shimizu, N. Quantum phase transition in the shape of zr isotopes. *Phys. Rev. Lett.* **117**, 172502 (2016). URL https://link.aps.org/doi/10.1103/PhysRevLett.117.172502. DOI 10.1103/PhysRevLett.117.172502.

18. Bree, N. *et al.* Shape coexistence in the neutron-deficient even-even $^{182-188}$Hg isotopes studied via coulomb excitation. *Phys. Rev. Lett.* **112** (2014). URL https://doi.org/10.1103%2Fphysrevlett.112.162701. DOI 10.1103/physrevlett.112.162701.

19. Marsh, B. *et al.* New developments of the in-source spectroscopy method at RILIS/ISOLDE. *Nucl. Instruments Methods Phys. Res. Sect. B: Beam Interactions with Mater. Atoms* **317**, 550–556 (2013). URL https://doi.org/10.1016%2Fj.nimb.2013.07.070. DOI 10.1016/j.nimb.2013.07.070.

20. Day Goodacre, T. *et al.* RILIS-ionized mercury and tellurium beams at ISOLDE/CERN. *Hyperfine Interactions* **238** (2017). URL https://doi.org/10.1007%2Fs10751-017-1398-6. DOI 10.1007/s10751-017-1398-6.

21. Wolf, R. *et al.* ISOLTRAP's multi-reflection time-of-flight mass separator/spectrometer. *Int. J. Mass Spectrom.* **349-350**, 123–133 (2013). URL https://doi.org/10.1016%2Fj.ijms.2013.03.020. DOI 10.1016/j.ijms.2013.03.020.

22. Brown, B. A. Double-octupole states in ^{208}Pb. *Phys. Rev. Lett.* **85**, 5300–5303 (2000). URL https://doi.

org/10.1103%2Fphysrevlett.85.5300. DOI 10.1103/physrevlett.85.5300.

23. Otsuka, T. *et al.* Novel features of nuclear forces and shell evolution in exotic nuclei. *Phys. Rev. Lett.* **104** (2010). URL https://doi.org/10.1103%2Fphysrevlett.104.012501. DOI 10.1103/physrevlett.104.012501.

24. Lettry, J. *et al.* Release from ISOLDE molten metal targets under pulsed proton beam conditions. *Nucl. Instruments Methods Phys. Res. Sect. B: Beam Interactions with Mater. Atoms* **126**, 170–175 (1997). URL https://doi.org/10.1016%2Fs0168-583x%2896%2901088-9. DOI 10.1016/s0168-583x(96)01088-9.

25. Lettry, J. *et al.* Effects of thermal shocks on the release of radioisotopes and on molten metal target vessels. *Nucl. Instruments Methods Phys. Res. Sect. B: Beam Interactions with Mater. Atoms* **204**, 251–256 (2003). URL https://doi.org/10.1016%2Fs0168-583x%2802%2901919-5. DOI 10.1016/s0168-583x(02)01919-5.

26. Fedosseev, V. *et al.* Ion beam production and study of radioactive isotopes with the laser ion source at ISOLDE. *J. Phys. G: Nucl. Part. Phys.* **44**, 084006 (2017). URL https://doi.org/10.1088%2F1361-6471%2Faa78e0. DOI 10.1088/1361-6471/aa78e0.

27. Rothe, S. *et al.* Narrow linewidth operation of the RILIS titanium: Sapphire laser at ISOLDE/CERN. *Nucl. Instruments Methods Phys. Res. Sect. B: Beam Interactions with Mater. Atoms* **317**, 561–564 (2013). URL https://doi.org/10.1016%2Fj.nimb.2013.08.058. DOI 10.1016/j.nimb.2013.08.058.

28. Wolf, R. N., Eritt, M., Marx, G. & Schweikhard, L. A multi-reflection time-of-flight mass separator for isobaric purification of radioactive ion beams. *Hyperfine Interactions* **199**, 115–122 (2011). URL https://doi.org/10.1007%2Fs10751-011-0306-8. DOI 10.1007/s10751-011-0306-8.

29. Wienholtz, F. *et al.* Towards ultra high-resolution multi-reflection time-of-flight mass spectrometry at ISOLTRAP. *Phys. Scripta* **T166**, 014068 (2015). URL https://doi.org/10.1088%2F0031-8949%2F2015%2Ft166%2F014068. DOI 10.1088/0031-8949/2015/t166/014068.

30. Sels, S. *In-source resonance-ionization spectroscopy of neutron-deficient* $^{177-185}Hg$ *isotopes* (In preparaton, 2018).

31. Bohr, A. & Mottelson, B. R. *Nuclear Structure* (World Scientific Publishing Company, 1998). URL https://doi.org/10.1142%2F3530-vol2.

32. Tsunoda, Y., Otsuka, T., Shimizu, N., Honma, M. & Utsuno, Y. Novel shape evolution in exotic ni isotopes and configuration-dependent shell structure. *Phys. Rev. C* **89**, 031301 (2014). URL https://link.aps.org/doi/10.1103/PhysRevC.89.031301. DOI 10.1103/PhysRevC.89.031301.

33. Berdichevsky, D. & Tondeur, F. Nuclear core densities isotope shifts, and the parametrization of the droplet model. *Zeitschrift für Physik A Atoms Nucl.* **322**, 141–147 (1985). URL https://doi.org/10.1007%2Fbf01412027. DOI 10.1007/bf01412027.

34. Day Goodacre, T. *Developments of the ISOLDE RILIS for radioactive ion beam production and the results of their application in the study of exotic mercury isotopes*. Ph.D. thesis, School of Physics and Astronomy, The University of Manchester (2016).

35. Sels, S. *Laser spectroscopy of mercury - Return towards sphericity*. Ph.D. thesis, Instituut voor Kern en Stralingsfysica, K.U. Leuven, B-3001 Leuven, Belgium (2018).

36. Reimann, R. J. & McDermott, M. N. Precision magnetic moment determinations for 43-min ^{199m}Hg and other isomers of mercury. *Phys. Rev. C* **7**, 2065–2079 (1973). URL https://link.aps.org/doi/10.1103/PhysRevC.7.2065. DOI 10.1103/PhysRevC.7.2065.

37. Kohler, R. H. Detection of double resonance by frequency change: Application to ^{201}Hg. *Phys. Rev.* **121**, 1104–1111 (1961). URL https://link.aps.org/doi/10.1103/PhysRev.121.1104. DOI 10.1103/PhysRev.121.1104.

Supplementary Information

The isotope shifts and corresponding $\delta\langle r^2 \rangle$ values are provided in Table 1. A complete description of the data analysis and fitting can be found in the Doctoral theses of T. Day Goodacre[34] and S. Sels[35]. The close agreement between the values extracted from this work with those of literature is a convincing validation of the data treatment.

Acknowledgements

Table 1. Summary of resulting mean-square charge differences ($\delta\langle r^2\rangle^{A-198}$) and nuclear moments ($\mu$, Q) and their comparison to literature.

Isotope	Spin I^π	$\delta\langle r^2\rangle^{A-198}$ (this work) (fm^2)	$\delta\langle r^2\rangle^{A-198}$ (lit.) (fm^2)	μ (this work) (μ_N)	μ (lit.) (μ_N)	Q_s (this work) (b)	Q_s (lit.) (b)
^{177}Hg	$(7/2^-)$	-1.067(8){78}	-	-1.027(53)	-	0.57(83)	-
^{178}Hg	0^+	-0.968(6){71}	-	-	-	-	-
^{179}Hg	$(7/2^-)$	-0.905(5){70}	-	-0.949(29)	-	0.77(28)	-
^{180}Hg	0^+	-0.808(5){60}	-	-	-	-	-
^{181}Hg	$1/2^-$	-0.111(6){11}	-0.114(4){10}	0.510(9)	0.5071(7)	-	-
^{182}Hg	0^+	-0.653(5){48}	-0.649(10){49}	-	-	-	-
^{183}Hg	$1/2^-$	-0.065(5){7}	-0.069(2){6}	0.516(11)	0.524(5)	-	-
^{184}Hg	0^+	-0.542(5){40}	-0.544(2){42}	-	-	-	-
^{185}Hg	$1/2^-$	-0.069(6){7}	-0.0764(6){63}	0.507(17)	0.509(4)	-	-
^{185m}Hg	$13/2^+$	-0.543(4){40}	-0.543(2){42}	-1.009(12)	-1.017(9)	-0.15(41)	0.19(32)

Statistical errors are given in parenthesis. Systematic errors stemming from
the indeterminacy of the F factor (7%, see[4]) and M$_{SMS}$ are shown in curly brackets
Ref. for μ: $\mu(^{199}$Hg$^m) = -1.0147(8)$, $a(^{199}$Hg$^m) = -2298.3(2)$[36]
Ref. for Q_s: $Q_s(^{201}$Hg$) = 0.387(6)$[2], $b(^{201}$Hg$) = -280.107(5)$[37]

Author contributions statement

A.A, A.B, T.D.G, D.V.F, V.N.F, L.P.G, M.H, B.A.M, M.D.S, P.V.D concieved the experiment and prepared the proposal; T.D.G, D.V.F, V.N.F, B.A.M, Y.M.P, P.L.M, R.E.R, S.R, M.V carried out laser ionization scheme and/or ion source developments; A.A, K.B, T.E.C, V.N.F, M.H, S.K, B.A.M, L.S, P.V.D, K.Z supervised the participants; B.A, N.A.A, D.A, A.B, J.B, T.E.C, J.G.C, T.D.G, G.J.F, D.V.F, V.N.F, K.T.F, L.P.G, L.G, M.H, K.M.L, V.M, B.A.M, Y.M.P, P.L.M, R.E.R, S.S, P.S, C.V.B, P.V.D, M.V, E.V, A.W, F.W, A.Z participated in data taking; T.O, Y.T peformed MCSM calculations; J.D, A.P peformed DFT calculations; A.B, T.D.G, D.V.F, B.A.M, P.L.M, R.E.R, S.R, M.V took part in laser set up and oper-ation; B.A, D.A, T.E.C, J.G.C, K.T.F, L.P.G, L.G, K.M.L, V.M, M.R, R.E.R, L.S, S.S, C.V.B, A.W, F.W, R.N.W set up and operated the detection and data acquisition systems; A.A, A.B, K.B, T.E.C, T.D.G, J.D, D.V.F, L.P.G, M.H, B.A.M, T.O, L.S, M.D.S, S.S, P.V.D, E.V, K.W contributed to the data analysis and interpretation; A.A, A.B, K.B, T.E.C, J.G.C, T.D.G, J.D, V.N.F, L.P.G, M.H, D.L, B.A.M, T.O, L.S, S.S, Y.T, P.V.D contributed to the manuscript preparation.